scientific reports

Check for updates

OPEN

Mathematical analysis of scrub typhus seasonal infection with re-scaled transmission rate considering Northeast India reported data from 2010 to 2022

Biplab Dhar[1] & Mohammad Sajid[2]✉

Healthcare reporting methods have seen a common problem with actual incidence of scrub typhus cases in Northeast India that were reported during post rainy season. We propose a Host-Vector model, a first of its kind, with a significant modification in the disease infection transmission rate. Our work aims to investigate a mathematical model by Atangana-Baleanu fractal-fractional operator that has seasonal pattern incorporating 2010–2022 data. The existence-uniqueness property is investigated using the fixed point theory, and also Ulam-Hyers stability is performed. Based on Lagrange's interpolation polynomial in the numerical scheme, a numerical investigation for various values of the fractional parameters is presented. The numerical simulation and phase plane trajectories demonstrates excellent performance of the suggested model as the number of individuals who recover rises gradually after herd immunity threshold points and turning points. Furthermore, the information gathered here may be useful for enhancing spatiotemporally dynamic scrub typhus disease models.

Keywords Tropical disease, Entomology, AB fractal-fractional derivative, Fractional parameters, Periodicity, Simulation

A neoteric mathematical scrub typhus disease model for a 13 years data-set from Northeast India having herd immunity threshold is presented in this article. In this section, we present background studies for the scrub typhus disease, then a brief literature survey of the disease in Northeast India and finally an illustrative impact on how mathematics (with fractional calculus) can be a helping hand in understanding the disease dynamics. According to a 2024 opinion by Mohapatra et al.[1], scrub typhus has drawn attention in India due to the thousands of reported cases and numerous deaths in 2023. The disease is one of the neglected tropical zoonotic diseases spread by vectors. The World Health Organization has recognised this infamous disease to be endemic in the Asia-Pacific area, also known as the "tsutsugamushi triangle"[2] (see Fig. 1). The disease is contracted by humans (called as hosts) from the bites of infected mites (called as vectors). Worldwide, scrub typhus is predicted to have impact over a million individuals annually and result in significant mortality rates[3]. In tropical regions, scrub typhus is year-round, but in temperate regions, it can only occur occasionally. This disease initially presents with symptoms that are similar to other infections, including dengue, encephalitis, influenza, corona viruses, etc. Hence, is difficult to diagnose, but a timely and accurate diagnosis could minimize complications and even prevent death. However, the disease has recently spread to urban areas. When people receive no treatment, the death rate can exceed 30%. Foreign scrub typhus cases have also been detected in some travellers who have returned from that triangle[4–7]. Diagnoses can be difficult in hilly areas where there are a lot of rural tribal populations. It is also crucial to evaluate many related factors, such as the ecology on the spread of scrub typhus in the region, which includes the rodent population, habitat features, and climate as per Konyak et al.[8]. The authors have tried to bring a paradigm shift that has never done before in formulating a fractional mathematical model depicting scrub typhus transmission with support of proper literature surveys.

Known for its distinct "slash and burn" farming method, Northeast India is a region in Southeast Asia. To foster the growth of scrub vegetation, this traditional method of farming entails clearing the forests. Because of this, the area becomes a perfect home for the mites that spread scrub typhus. Along with its rich biodiversity,

[1]Applied Science Cluster - Mathematics, UPES, Dehradun, UK, India. [2]Department of Mechanical Engineering, College of Engineering, Qassim University, Buraydah, Saudi Arabia. ✉email: msajd@qu.edu.sa

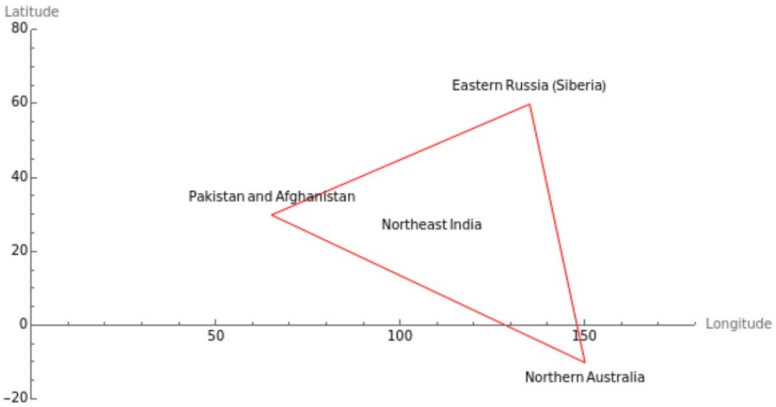

Fig. 1. Tsutsugamushi Triangle that shows the broad areas which are scrub typhus endemic, loosely drawn in Wolfram Mathematica.

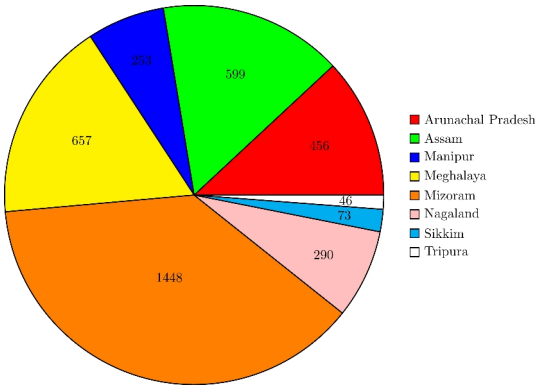

Fig. 2. Confirmed scrub typhus cases and visual representation of the disease burden in Northeast India from 2010 to 2022.

Northeast India is known for having a lot of these mites because of its lush vegetation[9]. Following the discovery of the initial episodes of the disease in Northeast India during World War II, about 91 cases were reported among military personnel between 1965 and 1969. But, there have been cases of febrile illnesses with eschar formation documented in several regions of Northeast India since 2001 after decades of decline in scrub typhus. Still, there is a dearth of precise information about the prevalence of scrub typhus across many Northeastern states[8].

Geographic variations in climatic conditions, the availability of a variety of aetiological agents, vectors associated with spread, human behaviours, and population susceptibility all influence the epidemiology of scrub typhus. Most patients had medically suspected instances of the illness when they first arrived, displaying symptoms like acute indistinguishable febrile illness and prolonged fever. The findings done by Konyak et al.[8] suggests that the months of Jul through Nov (rainy season or post-rain months) saw the greatest number of cases reported. The reported cases of Northeast India from 2010 to 2022 are tallied in the Fig. 2.

The trends and variations in infectious diseases such as influenza virus, AIDS, TB, HIV, Q-fever, age-specific smoke model, etc. have been studied with this method[10–16]. Based on data availability, these models carefully foresee and anticipate the onset of diseases and assess the effectiveness of various strategies, including medication, isolation, vaccination, and quarantine.

Researchers from all over the world are becoming more interested in fractional calculus because of its many benefits and useful applications[17]. Perhaps, according to Naik et al.[18], the only model that works well for researching memory, switching behavior, and genetic variation is one that has a fractional-order system. To quantify the fractal dimensions of real events, Atangana[19] developed "fractal-fractional differential and integral operators." The "Fractal-Fractional" operator (we call it as the F-F operator) is used to combine fractional differentiation with fractal derivative to perform a single differentiation when working with complex physical problems, such as those that exhibit fractal characteristics. Rather than following standard mathematical models, which usually depend on integer dimensions and continuous functions, these models adopt the idea of fractional dimensions. In the year 2022, Thiriot et al.[20] have established an in-apparent infection mouse model for scrub typhus using out-breed CD-1 mice. This model closely resembles natural infection by intra-dermal injection and it helped the researcher to analyze host predisposition, disease progression and host responses. This development also improved the knowledge of immune responses after skin exposure to Orientia tsutsugamushi and revealed future research to scrub typhus medication or/and prevention. The model is very important for

both acute as well as chronic phases of the disease and in the development of several potential therapeutic and preventive procedures. An analytical mathematical model was investigated by Shah et al.[21] to study the transmission of tungiasis infection that was modelled using the Atangana-Baleanu fractional derivative. It examined the interactions between people and sand fleas, taking into account the rates of infection, incubation, and recovery. The effect of management strategies and treatments on the prevalence of tungiasis was assessed using numerical simulations.

There are not very insights from mathematical modeling in scrub typhus dynamics, of which significant details for some are mentioned here. Starring with the year 2015, a prominent study regarding an investigation done by Kwak et al.[22] deals with building an incidence prediction model of scrub typhus in South Korea using climatic variables. The researchers applied the model for the period 2011-2012, and the results show the usefulness of the model in predicting the cases of scrub typhus. It also emphasized the necessity of seasonal leading of climatic conditions before the meteorological data is given a final conclusion that would give effective response for scrub typhus outbreak and management to the public health bureau. The study also recognised that although these meteorological factors may be seasonal there may not be a direct association between the seasonality of the factors and the scrub typhus outbreak events, and therefore caution should be taken when addressing the issue of seasonality so as to improve a model. Next, in the year 2018, the paper authored by Min et al.[23] described the growing tendencies of the rate of the development of scrub typhus in South Korea and possible reasons, which play an important role in climate change. Transmission parameters include rodent and mite numbers and their interaction frequency; high contact rates are stressed for controlling the overall disease transmission, especially human-mite contact. Subsequently, in 2019, an article by Yao et al.[24] studied spatial and temporal characteristics of scrub typhus in China considering environmental, socio-economic, and climatic variables. These factors are used to explain the likelihood of scrub typhus outbreaks stressing the importance of integrated risk reduction strategies. After two decades in 2021, the work done by Bondarenko et al.[25] gave an evaluation of the time series of scrub typhus occurrences in Thailand. The authors concerned the detection of a relationship between metrical factors and disease occurrences, with emphasis made on the temperature and humidity. The findings indicate that using the weather data enhances the extent of the forecast, supporting the applicability of the methods in the planning and preparation for the future health risks. Recently, on Jan 2024, a study done by D'Cruz et al.[26] on scrub typhus in Vellore, Tamil Nadu, it was determined that the months of the year that the disease vector was most active were between Aug and Feb with the highest incidences in the month of Oct and Nov. A month later, by Feb 2024, Peng et al.[27] has done a study on scrub typhus in China over 51 years. Highest rates were recorded during the periods of May to Nov mostly amongst the peasants and farmers. Thus, changes in the environment, as well as the growing trend in population for urbanization play a major role in the rising cases. The authors believe that these key insights are also applicable to Northeast India and hence, have to recommend aggressive and effectively timed public health interventions during peak seasons. From the point of view of a latest research by Lynnette et al.[28], diagnostics for scrub typhus in the current world mainly serological based are not efficient and requires improvement through molecular based tests such as PCR and LAMP. It highlights the need to establish the point-of-care testing in the low-resource centre and foremost the review of the clinical algorithm with laboratory tests enhances the overall perception of the diagnosis and the treatment of the diseases. Thus, this research could be useful in mathematical modeling of scrub typhus occurrence and diagnosing the disease as it reveals the overall experience in the epidemiology, clinical manifestations, and diagnosis of the given disease. The combination of findings based on empirical studies and mathematical simulations can help to fine-tune the existing guidelines for diagnosing and managing patients with diseases that are prevalent in some regions, which in turn would enhance the population's health. The main contributions of this paper are listed as follows:

i) A real data-set of recovered people is considered from year 2010 to 2022 in which we have assumed total number of infections as 10,000.
ii) Relapse cases of scrub typhus is common[29] and therefore we have formulated an F-F model including memory effect.
iii) The reproduction number is taken as time-dependent which is frequently considered as a constant number.

The remaining parts of the article are catalogued as follows: To understand the F-F operator, definitions are provided in the Sect. 2. A model is proposed detailing motivation, assumptions and formulation. We have also given possible biological significance of fractional parameters: fractional order m and fractal dimension n, there. The qualitative analysis of model: existence-unicity, non-negativity and boundedness of solution is attempted together with Ulam-Hyers stability. The co-existing equilibrium point is evaluated and also presented its biological interpretation. A brief note on seasonal variation effects is done which is followed by numerical simulation. The numerical results are depicted in Sect. 3 with thorough interpretation and discussion. At the end, we have written a conclusion in Sect. 4.

Materials and methods

A few basic definitions relevant to F-F operators are covered in this section[19,30]. We made an assumption that $\{\mathbb{X}(t) \in \mathcal{C}([0,1]) \to \mathbb{R}\}$ with a norm defined as $\| \mathbb{X}(t) \| = \max_{t\in[0,1]} | \mathbb{X}(t) |$.

Definition 1 Let $\mathbb{X}(t) \in (x_1, x_2)$ be a fractional differentiable smooth curve is present in the sense $0 < m < 1$ and $0 < n \leq 1$, then F-F Atangana-Baleanu (AB) derivative sense with generalized "Mittag-Leffler" (M-L) kernel

$$^{ff}\mathcal{D}^{m,n}_{x_1,t}\mathbb{X}(t) = \frac{\mathcal{N}(m)}{1-m}\frac{d}{dt^n}\int_{x_1}^{t}\mathbb{X}(s)\mathcal{E}_m\left[-\frac{m}{1-m}(t-s)^m\right]ds,$$

where $\mathcal{N}(m) = 1 - m + \frac{m}{\Gamma(m)}$ is called normalization map satisfying $\mathcal{N}(0) = \mathcal{N}(1) = 1$, can be generalized into

$$^{ff}\mathcal{D}^{m,n,a}_{x_1,t}\mathcal{F}(t) = \frac{\mathcal{N}(m)}{1-m}\frac{d^a}{dt^n}\int_{x_1}^{t}\mathcal{F}(s)\mathcal{E}_m\left[-\frac{m}{1-m}(t-s)^m\right]ds,$$

where $a \in (0, 1]$. Here, $\frac{d\mathbb{X}(s)}{ds^n} = \lim_{b\to s}\frac{\mathbb{X}(b)-\mathbb{X}(s)}{b^n - s^n}$.

Definition 2 The F-F AB integral for $\mathbb{X}(t)$ with M-L kernel is given by

$$^{ff}\mathcal{I}^{m,n}_{x_1,t}\mathbb{X}(t) = \frac{n(1-m)t^{n-1}}{\mathcal{N}(m)}\mathbb{X}(t) + \frac{mn}{\mathcal{N}(m)\Gamma(m)}\int_{x_1}^{t}(t-s)^{m-1}s^{n-1}\mathbb{X}(s)ds.$$

It can be easily understood that by pluging $n = 1$, the F-F derivative $^{ff}\mathcal{D}^{m,n}_{x_1,t}$ is the standard RL derivative $^{RL}\mathcal{D}^{m}_{x_1,t}$ of fractional order *m* in AB sense.

Definition 3 The RL derivative in AB sense for the function $\mathcal{X}(t)$ with M-L kernel is given by

$$^{RL}\mathcal{D}^{m}_{x_1,t}\mathcal{X}(t) = \frac{\mathcal{N}(m)}{1-m}\frac{d}{dt}\int_{x_1}^{t}\mathcal{X}(s)\mathcal{E}_m\left[-\frac{m}{1-m}(t-s)^m\right]ds.$$

A promising avenue with many benefits is the use of F-F operator with double F&F orders in scientific research. This method captures complex patterns and irregularities that traditional methods might miss, allowing for a more sophisticated and strengthened representation of intricate systems by utilizing the two orders. The combination of fractional calculus and fractal geometry allows for more realistic analysis and modeling of real-life events, reflecting the intrinsic identical structures and fractional order dynamics with greater precision. This helps us better understand complex processes and create more reliable mathematical models that are applicable to a wide range of fields.

Remark 1 For sake of easiness, we consider $\frac{\mathcal{N}(m)}{1-m} = P(m)$ and $\frac{m}{\mathcal{N}(m)\Gamma(m)} = Q(m)$.

The model

A modified SIR model is hot off the press suggested by Kalachev et al.[31] targeting the COVID-19's not-reported cases in Missoula. We seek help of that study to propose our model together with more understandings in the realm of modeling vector-borne diseases that have some important findings relevant to the topic from neoteric researches.

Motivation

Recently, in the year 2023, Shocket et al.[32] concentrated on the aspects of quantifying and modeling the impacts of climate in determining mosquito borne diseases. It also debates the effects of temperature and rainfall on the disease transmission using nonlinear functions and noted that they are function of context. Giménez-Mujica et al.[33] proposed a methodology for estimating the ultimate shape of a vector-borne epidemic transmitted by Aedes aegypti such as Dengue, Chikungunya, or Zika. The approach was extended to to larger geographic areas by generalizing it to meta-population models. To capture the main elements of disease transmission and response, Young et al.[34] have introduced a framework which contains several levels of hierarchy. This framework provides the information on the factors that influence invasion success. In the year 2024, Gao et al.[35] offered many substantive findings in the mathematical fields such as merging the Lagrangian methods with epidemiologic models for vector counting. In another study, Wang et al.[36] conducted an investigation where the effect of Fokker-Planck-type diffusion of a vector-borne disease in relation to the spread and control measures taken, focusing on effects due to spatial heterogeneity. Anwar et al.[37] augmented a mathematical model for understanding of the progression of Plasmodium vivax that can help design more efficient means of controlling and eradicating the same. The study stressed on the inclusion of delay differential equations, spatial data, etc., in addition to the integration of geo-data in the models to improve the model's practicality for the intervention programs in disease control, especially in public health. Ferraguti et al.[38] brought out the importance of the presence of the mosquito species identity in quantitative model of vector-borne diseases, as different species have different abilities of pathogen transmission. Species-specific vector competence, ecological interactions, temporal and spatial scales, and control strategies evaluation are also incorporated in that model. In Qiang et al.[39], the authors presented a study on an almost periodic reconstruction of vector-borne diseases in context to an environment that may be predictable but non-constant.

Parameters:	ω_1	ω_2	k_1	k_2	k_3	k	ρ_1	ρ_2	β	η
Values:	8	200	$\frac{1}{2}$	$\frac{1}{2}$	$\frac{4}{5}$	$\frac{2}{5}$	$\frac{1}{25000}$	20	$\frac{1}{5000}$	2

Table 1. The parameter values of system (1) for point of reference estimated from Min et al.[23] and Saha et al.[40].

	All infections: 10,000 humans	
	Symptomatic (95%): 9500 humans	**Asymptomatic (5%): 500 humans**
Attending healthcare	Yes (60%): 5700	No (40%): 3800
Diagnosed correctly	Yes (67%): 3820	No (33%): 1880
Reported	Yes: 3820	No: 1880
Fraction of infections	$u = 0.95 \times 0.6 \times 0.67 = 0.382$	$\bar{u} = 1 - u = 1 - 0.382 = 0.618$
	Cases reported: 3820 cases[8]	Cases not-reported: $1880 + 3800 + 500 = 6180$

Table 2. An example is provided to show the cases from Northeast India that are reported in health systems between 2010 and 2022, as well as the cases that are overlooked.

Assumptions and formulation

We have considered a scrub typhus infection incorporating human-mites relationship with humans as dead-end hosts and mites as disease spreading vectors. The host population is fragmented into three disjoint compartments, namely host-susceptible populations $S(t)$, host-infected populations $I(t)$ and host-recovered populations $R(t)$ at any time t. The vectors population at that same time t is denoted by $V(t)$.

$$\begin{aligned} {}^{ff}\mathcal{D}_{0,t}^{m,n} S(t) &= \omega_1 - (1-k_1)\,\bar{\beta} S(t) V(t) - \rho_1 S(t), \\ {}^{ff}\mathcal{D}_{0,t}^{m,n} I(t) &= (1-k_1)\,\bar{\beta} S(t) V(t) - \eta k_2 I(t) - \rho_1 I(t), \\ {}^{ff}\mathcal{D}_{0,t}^{m,n} R(t) &= \eta k_2 I(t) - \rho_1 R(t), \\ {}^{ff}\mathcal{D}_{0,t}^{m,n} V(t) &= \omega_2 - k k_3 V(t) - \rho_2 V(t), \end{aligned} \tag{1}$$

with initial conditions given by $(S(0), I(0), R(0), V(0)) \geq 0$. Further speculations on the proposed model are given as follows:

i) Host-susceptibles and vectors are recruited in the system with rates ω_1 and ω_2, respectively.
ii) Rate of infection transmission for host-susceptibles is taken unidirectional.
iii) Normal death rates of hosts and vectors are supposed to be ρ_1 and ρ_2, respectively.
iv) Three different measures are taken, namely protection measure against mites k_1 for host-susceptibles, treatment measure k_2 for host-infecteds, and mites killing efforts by humans k_3 with $k_{\phi=1,2,3} \in (0,1] \subset \mathbb{R}$.
v) The vector killing efficiency rate is denoted by k.
vi) Infection transmission rate of the compartment $I(t)$ is $(1-k_1)\,\bar{\beta} SV$, where $\bar{\beta} = \dfrac{\beta}{u}$ is re-scaled rate of infection transmission to host-susceptible. It should be noted that vectors are not infected after biting the infected hosts.
vii) Rate of host recovery from infection is η.

The parameters considered are positive and tabulated in Table 1.

Using the proposed modified SIRV model, we can estimate the fraction of reported cases for infectious diseases by introducing a crucial parameter u called the "reporting parameter". The under-reporting fraction $\bar{u}$, or the percentage of all infections that a health system somehow missed, can then be found using the formula $\bar{u} = 1 - u$. Assumed cases are those who sought medical attention, presented with symptoms, and received a proper diagnosis (refer to a case in Table 2). We use simulated data with known u values that is, the proportion of cases that are reported to demonstrate the methodology. In this instance, 95% of all infected people develop symptoms; of these, 60% visit a doctor, and 67% are reported via the notification system. The parameter u is equal to 0.382, or 3820 reported cases of infection, if the total (true) number of infections was 10,000. It is crucial to stress that the only coefficient u that can be estimated is the combined effect of the illness surveillance pyramid stages. Usually, the data at hand does not allow for the distinct effects of individual stages to be explained.

Biological significance of fractional parameters

Situation with short-term diseases, such as scrub typhus, the mentioned concept of the F-F derivative involves its usage depending on the specific disease's features and the type of processes affecting the infection transmission and development. For instance, if disease spread depends on the lower past numbers of contacts and exposures, coordinated in the last few days or weeks, fractional derivatives are more relevant to modeling than standard ones. It is then possible to refine the model's predictions of the future course of the outbreak by including

memory effects in the contact patterns and changes in the environment. This as far as disease transmission is concerned means that *m* explains how previous infection and precaution rates determine the current status of the disease; it signifies that the spread of the pathogen and the response of the population are not abrupt actions of the present but actions in the light of past events and conditions. Fractional diffusion as is explained through *n* shows that the effects of the disease do not decay exponentially but rather follow a more complicated history dependent process. It incorporates the variation in the time-scale of recovery between people and perhaps in the efficacy of medical treatments across time.

Model analysis

This section examines and deals in the solution's qualitative analysis such as existence-uniqueness, non-negativity, and boundedness properties.

Existence and unicity of solution

The system (1) can be re-written in matrix form as:

$$\begin{aligned} {}^{ff}\mathcal{D}_{0,t}^{m,n}\mathfrak{G}(t) &= \mathfrak{F}\left(t,\mathfrak{G}(t)\right), \\ &= \left(\Gamma_i\left(t,\mathfrak{G}(t)\right)\right)_{i=1}^{4}, \end{aligned} \tag{2}$$

where $\mathfrak{G}(t) = (S(t), I(t), R(t), V(t))$. A Banach space is now defined as $\mathfrak{U} = \mathcal{X}^4$, where the algebraic structure of $\mathcal{X}$ is $\mathcal{C}\left(\mathcal{I} = [0,t], \mathbb{R}\right)$ and the norm equipped is given by $\| h \| = \max_{t\in[0,1]} |S(t) + I(t) + R(t) + V(t)|$ such that

$$\mathfrak{F}(t) = \mathfrak{F}(0) + nQ(m)\int_0^t s^{n-1}(t-s)^{m-1}\mathfrak{F}(s,\mathfrak{G}(s))ds + \frac{nt^{n-1}\mathfrak{F}(t,\mathfrak{G}(t))}{P(m)}.$$

Let us consider $\| S(t) \| \leq c_1$, $\| I(t) \| \leq c_2$, $\| R(t) \| \leq c_3$ and $\| V(t) \| \leq c_4$ for some constants $c_{\phi=1,2,3,4} > 0$. In this scenario, the F-F system (1) can be transformed into RL derivative system in AB sense as follows:

$$\begin{aligned} {}^{RL}\mathcal{D}_{0,t}^{m}S(t) &= nt^{n-1}\Gamma_1(t,\mathfrak{G}(t)), \\ {}^{RL}\mathcal{D}_{0,t}^{m}I(t) &= nt^{n-1}\Gamma_2(t,\mathfrak{G}(t)), \\ {}^{RL}\mathcal{D}_{0,t}^{m}R(t) &= nt^{n-1}\Gamma_3(t,\mathfrak{G}(t)), \\ {}^{RL}\mathcal{D}_{0,t}^{m}V(t) &= nt^{n-1}\Gamma_4(t,\mathfrak{G}(t)), \end{aligned}$$

where

$$\begin{aligned} \Gamma_1(t,\mathfrak{G}(t)) &= \omega_1 - (1-k_1)\,\bar{\beta}S(t)V(t) - n_1S(t), \\ \Gamma_2(t,\mathfrak{G}(t)) &= (1-k_1)\,\bar{\beta}S(t)V(t) - \eta k_2 I(t) - n_1 I(t), \\ \Gamma_3(t,\mathfrak{G}(t)) &= \eta k_2 I(t) - n_1 R(t), \\ \Gamma_4(t,\mathfrak{G}(t)) &= \omega_2 - kk_3V(t) - n_2V(t). \end{aligned}$$

After the application of fractional integrals, we have

$$\mathfrak{F}(t) = \mathfrak{F}(0) + nQ(m)\int_0^t s^{n-1}(t-s)^{m-1}\mathfrak{F}(s,\mathfrak{G}(s))ds + \frac{nt^{n-1}\mathfrak{F}(t,\mathfrak{G}(t))}{P(m)}.$$

It must be noted that the function $\mathfrak{F}(t,\mathfrak{G}(t))$ must meet increasing and Lipschitz conditions.

Theorem 1 *For every $\mathfrak{G}_{\phi=1,2} \in \mathfrak{B}$, where $\mathfrak{B}$ is a Banach space, there exist a positive real number c that satisfies*

$$\| \sum_{\phi=1}^{2}(-1)^{\phi+1}\mathfrak{F}(t,\mathfrak{G}_\phi)(t) \| \leq c \,|\sum_{\phi=1}^{2}(-1)^{\phi+1}\mathfrak{G}_\phi(t)|, \tag{3}$$

where $c = max\left\{\rho_1, b_{\phi=1,2,3}\right\}$ with $b_1 = 2(1-k_1)\bar{\beta}c_2 + \rho_1$, $b_2 = 2\eta k_2 + \rho_1$ and $b_3 = 2(1-k_1)\bar{\beta}c_1 + kk_3 + \rho_2$.

Proof As per the statement, for every $\mathfrak{G}_{\phi=1,2} \in \mathfrak{B}$, we get

$$\begin{aligned} \| \sum_{\phi=1}^{2}(-1)^{\phi+1}\mathfrak{F}(t,\mathfrak{G}_\phi)(t) \| &\leq b_1|S_1 - S_2| + b_2|I_1 - I_2| + \rho_1|R_1 - R_2| + b_3|V_1 - V_2| \\ &\leq c \,|\sum_{\phi=1}^{2}(-1)^{\phi+1}\mathfrak{G}_\phi(t)|. \end{aligned}$$

This shows that the Lipschitz condition is satisfied by function $\mathfrak{F}(t, \mathfrak{G}(t))$. □

Theorem 2 *For every* $\mathfrak{G} \in \mathfrak{B}$, *there exists constants* $c_{\mathfrak{G}}$ *and* $W_{\mathfrak{G}}$ *such that*

$$|\mathfrak{F}(t, \mathfrak{G}(t))| \leq c_{\mathfrak{G}}|\mathfrak{G}(t)| + W_{\mathfrak{G}}.$$

Therefore, there is minimum one solution to our proposed system (1).

Proof First, we show that the function $\mathfrak{F}$ given in system (2) is completely continuous. Since, sum total of all state variables $N = S(t) + I(t) + R(t) + V(t)$ is continuous because $\mathfrak{G}$ is continuous. □

Theorem 3 *Let us consider that the Inequation* (3) *is true, then for*

$$\Theta = \left(\frac{nt^{n-1}}{P(m)} + nQ(m)T^{m+n-1}\mathfrak{H}(m,n) \right) c,$$

the system (1) has a unique solution.

Proof For $\mathfrak{G}_1, \mathfrak{G}_2 \in \mathfrak{B}$, we get

$$\begin{aligned}
|\sum_{\phi=1}^{2}(-1)^{\phi+1}h(\mathfrak{G}_\phi)| = \max_{t\in[0,T]} |&\frac{nt^{n-1}}{P(m)}\sum_{\phi=1}^{2}(-1)^{\phi+1}\mathfrak{F}(t,\mathfrak{G}_\phi(t)) \\
&+ \frac{mn}{\mathcal{N}(m)}\int_0^t s^{n-1}(t-s)^{m-1}\sum_{\phi=1}^{2}(-1)^{\phi+1}\mathfrak{F}(s,\mathfrak{G}_\phi(s)ds| \\
&\leq c\left[\frac{nt^{n-1}}{P(m)} + \frac{mn}{\mathcal{N}(m)\Gamma(m)}T^{m+n-1}\mathfrak{H}(m,n)\right] \times \parallel \mathfrak{G}_1 - \mathfrak{G}_2 \parallel \\
&\leq \Theta \parallel \mathfrak{G}_1 - \mathfrak{G}_2 \parallel .
\end{aligned}$$

For this reason, the function h is a contraction and there exists only a solution for the system (1). □

Non-negativity and boundedness of solutions
A theorem is provided to glance upon this property pondering a hyperplane[41].

Theorem 4 *Solutions of the proposed model* (1), *which initiate at* $\mathbb{R}^4_+$, *are non-negative and bounded uniformly*.

Proof From the model (1), it can be seen that

$$\begin{aligned}
{}^{ff}\mathcal{D}_{0,t}^{m,n}S(t)|_{S=0} &= \omega_1 \ > 0, \\
{}^{ff}\mathcal{D}_{0,t}^{m,n}I(t)|_{I=0} &= (1-k_1)\bar{\beta}S(t)V(t) \ \geq 0, \\
{}^{ff}\mathcal{D}_{0,t}^{m,n}R(t)|_{R=0} &= 0, \\
{}^{ff}\mathcal{D}_{0,t}^{m,n}V(t)|_{V=0} &= \omega_2 \ \geq 0.
\end{aligned} \tag{4}$$

As per this, if $(S(0), I(0), R(0), V(0)) \in \mathbb{R}^4_+$, the solution cannot run away from the hyperplane. Also, the collection of points of vector field into $\mathbb{R}^4_+$ is a non-negative invariant set captivating all orthant on each hyperplane. □

Ulam-Hyers stability
Stability is an important topic in the qualitative theory of differential equations. Many stability types, including exponential, Lyapunov, asymptotic, and others, can be found in several literatures. But in terms of optimization and numerics, Ulam-Hyers (U-H) stability[42] is the most important type of stability because it provides a connection between the exact and numerical solutions.

Definition 4 The model (1) is said to be U-H stable if for each $(\mathrm{S}, \mathrm{I}, \mathrm{R}, \mathrm{V}) \in \mathcal{B}$ there exists $h_{\phi=1,2,3,4} > 0$ such that a real number $\mathcal{W}_{\phi=1,2,3,4} > 0$ is defined satisfying the set of inequalities

$$\begin{aligned}
|^{ff}\ \mathcal{D}_{0,t}^{m,n}\mathrm{S}(t) - \mathcal{M}_1(\mathrm{S},t)\ | &\leq \mathcal{W}_1, \\
|^{ff}\ \mathcal{D}_{0,t}^{m,n}\mathrm{I}(t) - \mathcal{M}_2(\mathrm{I},t)\ | &\leq \mathcal{W}_2, \\
|^{ff}\ \mathcal{D}_{0,t}^{m,n}\mathrm{R}(t) - \mathcal{M}_3(\mathrm{R},t)\ | &\leq \mathcal{W}_3, \\
|^{ff}\ \mathcal{D}_{0,t}^{m,n}\mathrm{V}(t) - \mathcal{M}_4(\mathrm{V},t)\ | &\leq \mathcal{W}_4,
\end{aligned} \tag{5}$$

Also, for any time t there exists $(\mathcal{S}(t), \mathcal{I}(t), \mathcal{R}(t), \mathcal{V}(t))$ such that

$$
\begin{aligned}
f\left(\mathcal{S}(t)-\mathrm{S}\right) &\leq h_1\mathcal{W}_1,\\
f\left(\mathcal{I}(t)-\mathrm{I}\right) &\leq h_2\mathcal{W}_2,\\
f\left(\mathcal{R}(t)-\mathrm{R}\right) &\leq h_3\mathcal{W}_3,\\
f\left(\mathcal{V}(t)-\mathrm{V}\right) &\leq h_4\mathcal{W}_4.
\end{aligned}
$$

Here, the set $\mathcal{B}$ is the collection of all state variables output in $\mathbb{R}_+^4$ including the initial conditions, $f:[0,\infty)\times\mathbb{R}_+^4\to\mathbb{R}$ is a map defined by $f(S,I,R,V)=\max_{t\in[0,\infty)}\{|S|+|I|+|R|+|V|\}$, and $\mathcal{M}_1=\omega_1-(1-k_1)\,\bar{\beta}S(t)V(t)-\rho_1S(t)$, $\mathcal{M}_2=(1-k_1)\,\bar{\beta}S(t)V(t)-\eta k_2I(t)-\rho_1I(t)$, $\mathcal{M}_3=\eta k_2I(t)-\rho_1R(t)$, $\mathcal{M}_4=\omega_2-kk_3V(t)-\rho_2V(t)$.

Remark 2 S be a solution of the first inequality present in (5) if and only if there exists smooth curve $\mathcal{A}_1$ such that

i. $|\mathcal{A}_1|\leq\mathcal{W}_1$,
ii. ${}^{ff}\mathcal{D}_{0,t}^{m,n}\mathrm{S}(t)=\mathcal{M}_1+\mathcal{A}_1$.

In the same manner, appropriate smooth curves for the state variables I, R, and V can be found.

Theorem 5 *The model* (1) *is U-H stable if*

$$
\delta_\phi\left[\frac{nQ(m)\left\{\Gamma(m)\right\}^2}{\Gamma(m+n)}+\frac{n}{P(m)}\right]\leq 1, \tag{6}
$$

where $\phi=1,2,3,4$ and corresponding δ_ϕ are functions of h_ϕ respectively assigned for *S*, *I*, *R* and *V*.

Proof Let, $\mathrm{S}(t)$ and $\mathcal{W}_1$ be both positive. Therefore, $|{}^{ff}\mathcal{D}_{0,t}^{m,n}\mathrm{S}(t)-\mathcal{M}_1(\mathrm{S},t)|\leq\mathcal{W}_1$. Using the Remark 2(ii), it can be followed that

$$
{}^{ff}\mathcal{D}_{0,t}^{m,n}\mathrm{S}(t)=\mathcal{M}_1+\mathcal{A}_1. \tag{7}
$$

Employing AB integral (see Defn. 2) to the Eq. (7) gives

$$
\begin{aligned}
\mathrm{S}(t)-S(0)=&nQ(m)\int_0^t(t-l)^{m-1}\,l^{n-1}\mathcal{M}_1\left(l,\mathrm{S}(l)\right)dl+\frac{n}{P(m)}t^{n-1}\mathcal{M}_1\left(l,\mathrm{S}(t)\right)\\
&+nQ(m)\int_0^t(t-l)^{m-1}\,l^{n-1}\mathcal{A}_1(l)dl+\frac{n}{P(m)}t^{n-1}\mathcal{A}_1.
\end{aligned}
$$

Suppose $\mathcal{S}$ is a distinct solution for the model (1), then we have

$$
\mathcal{S}(t)-S(0)=nQ(m)\int_0^t(t-l)^{m-1}\,l^{n-1}\mathcal{M}_1\left(l,\mathcal{S}(l)\right)dl+\frac{n}{P(m)}t^{n-1}\mathcal{M}_1\left(l,\mathcal{S}(t)\right).
$$

This implies that

$$
\begin{aligned}
f\left(\mathrm{S}(t)-\mathcal{S}(t)\right)\leq&nQ(m)\int_0^t(t-l)^{m-1}\,l^{n-1}\mid\mathcal{M}_1\left(l,\mathrm{S}(l)\right)-\mathcal{M}_1\left(l,\mathcal{S}(l)\right)dl\mid\\
&+\frac{n}{P(m)}t^{n-1}\mid\mathcal{M}_1\left(l,\mathrm{S}(l)\right)-\mathcal{M}_1\left(l,\mathcal{S}(l)\right)dl\mid+\frac{n}{P(m)}t^{n-1}\mid\mathcal{A}_1\mid\\
&+nQ(m)\int_0^t(t-l)^{m-1}\,l^{n-1}\mid\mathcal{A}_1(l)\mid dl,\\
\leq&\delta_\phi\left[\frac{nQ(m)\left\{\Gamma(m)\right\}^2}{\Gamma(n+m)}+\frac{n}{P(m)}\right]f\left(\mathrm{S}(t)-\mathcal{S}(t)\right)\\
&+\left[\frac{nQ(m)\left\{\Gamma(m)\right\}^2}{\Gamma(n+m)}+\frac{n}{P(m)}\right]\mathcal{W}_1.
\end{aligned}
$$

Arranging further, it can be found that

$$
f\left(\mathrm{S}(t)-\mathcal{S}(t)\right)\leq\frac{\left[\frac{nQ(m)\left\{\Gamma(m)\right\}^2}{\Gamma(n+m)}+\frac{n}{P(m)}\right]\mathcal{W}_1}{1-\delta_\phi\left[\frac{nQ(m)\left\{\Gamma(m)\right\}^2}{\Gamma(n+m)}+\frac{n}{P(m)}\right]}.
$$

Upon the consideration of

$$h_1 \leq \frac{\left[\frac{nQ(m)\{\Gamma(m)\}^2}{\Gamma(n+m)} + \frac{n}{P(m)}\right]}{1-\delta_\phi\left[\frac{nQ(m)\{\Gamma(m)\}^2}{\Gamma(n+m)} + \frac{n}{P(m)}\right]}$$

yields $f(\mathrm{S}(t)-\mathcal{S}(t)) \leq h_1\mathcal{W}_1$. In the same manner, it is possible to have $h_{\phi=2,3,4}$ such that for the remaining variables the expressions $f(\mathrm{E}(t)-\mathcal{E}(t)) \leq h_2\mathcal{W}_2$, $f(\mathrm{V}(t)-\mathcal{V}(t)) \leq h_3\mathcal{W}_3$ and $f(\mathrm{I}(t)-\mathcal{I}(t)) \leq h_4\mathcal{W}_4$ are true. Thus, it can be said that model (1) is U-H stable. □

Co-existing equilibrium point and its biology

The coexistence fixed point in the SIRV model has a biological meaning of a stable state of disease existence but within a population with implications on disease control, intervention measures, and population long term dynamics.

The system (1) has only one equilibrium point where all the state variables co-exist and thus we call this point as co-existing equilibrium (CoE) point. We set the rate of change of state variables to zero to get a system of non-linear equations as follows:

$$\begin{aligned}
\omega_1 - (1-k_1)\bar{\beta}S(t)V(t) - \rho_1 S(t) &= 0,\\
(1-k_1)\bar{\beta}S(t)V(t) - \eta k_2 I(t) - \rho_1 I(t) &= 0,\\
\eta k_2 I(t) - \rho_1 R(t) &= 0,\\
\omega_2 - kk_3 V(t) - \rho_2 V(t) &= 0.
\end{aligned}$$

Solving which we get CoE point given by $P^*(S^*, I^*, R^*, V^*)$, where each of the components are as follows:

$$S^* = \frac{\omega_1(kk_3+\rho_2)}{\rho_1(kk_3+\rho_2)+\bar{\beta}\omega_2(1-k_1)}, I^* = \frac{\bar{\beta}\omega_1\omega_2(1-k_1)}{(\rho_1+\eta k_2)\left\{\rho_1(kk_3+\rho_2)+\bar{\beta}\omega_2(1-k_1)\right\}},$$
$$R^* = \frac{\bar{\beta}\eta\omega_1\omega_2 k_2(1-k_1)}{\rho_1(\rho_1+\eta k_2)\left\{\rho_1(kk_3+\rho_2)+\bar{\beta}\omega_2(1-k_1)\right\}}, V^* = \frac{\omega_2}{kk_3+\rho_2}.$$

Remark 3 The CoE point P^* is stable if $\left(kk_3\rho_1+\rho_1\rho_2+\bar{\beta}\omega_2\right)\left(\bar{\beta}k_1\omega_2\right)^{-1} > 1$. Therefore, we call the expression in the left hand side of this inequality as reproduction number denoted by

$$\mathcal{R}_0 = \frac{kk_3\rho_1+\rho_1\rho_2+\bar{\beta}\omega_2}{\bar{\beta}k_1\omega_2}.$$

At the CoE, the disease is not wiped out, but its occurrence becomes relatively constant in such a population. This means that the infection remains constant in the hosts and vectors as a feature of the disease. From the practical point of view, there are still vulnerable people and an endless percentage of infected or recovered persons. The transmitting population sustains a constant-level of transmission rate among the vectors of the disease. This equilibrium represents a status between rate of new infections and people recovering from the disease. The infection and the recovery rates are directly proportional, so that the size of the infected population is constant. For vector born diseases such as scrub typhus, the equilibrium means that people continue to be bitten by vectors who continue to spread the diseases with equal intensity while people who fall sick or die are replaced by new people to allow the vectors to continually spread the disease. In point of view of public health, the coexisting equilibrium is significant because it is the minimum level of control needed for the disease. When the force of infection is constant or reaches a steady state people continue to get infected, spread the disease with or without signs or symptoms, and do not get medical help through vector control, vaccination or treatment. It may also mean that random fluctuations, such as the season or some other environmental factor, can temporarily upset this balance but that, if you do not interfere with the system, it will regain this state.

Vectors like mites in diseases like scrub typhus remain a source of continual infection at the equilibrium assisting in the sustenance of the disease. The combined equilibrium implies that an infected human is in contact with the vector perpetually. This proves that any means of reducing the rate of reproduction among vectors can help one to shift the system from the stable state and towards the dark region implying the ultimate disease - free situation. Biological relevance of this equilibrium also assists in developing the right strategies on balance. For example, improving the vectors for transmission control or, increasing resistance by vaccination alters the dynamics of the field and results in lower prevalence of disease.

Seasonal variation effects

We examine how seasonal variation affects scrub typhus dynamics in this section. In general, seasonal rainfall raises the number of mite breading sites-that is, the mite population. However, due to the intricate interactions between climate conditions, humidity levels below 70% may reduce the mite population. Because the rates of transmission between humans and mites depend on the season, seasonal variation is incorporated into our

model in this instance. There is only one vector-to-host transmission rate, β, in our suggested model (1)[26]. It is assumed to vary sinusoid in nature and has a time period T. The exposed and infected population will rise at some specific values that are equivalent to the seasonal variation of β. For instance, during the rainy season (high mite activity), β rises hence more infections occur. In the dry season the function β reduces and thus the number of actual new cases reduces. In order to include the seasonal variations in system (1), the definition of the transmission rate β is modified as follows:[43]

$$\beta(t) = \beta_0 \left[1 + k_4 sin\left(\frac{2\pi\alpha t}{T}\right)\right], \tag{8}$$

where α is a positive constant, k_4 is the amount of seasonal variation force in humans, β_0 is the initial transmission rate in humans, and T is the total time-period. We assume $T = 120$, the periodic cycle in the above Eq. (8) signify a shorter seasonal cycle of roughly 120 days. This could be considered as targeting one particular season or period within a year that indicates prospectively higher rates of transmittance of the disease such as the monsoon or post monsoon season which generally spans about 4 months (July up to November). This is particularly useful in predicting intra-seasonal outbreaks, and short-term planning of public health interventions.

The seasonal variations in regions affected by scrub typhus are modeled in Fig. (3) where the transmission rate $\beta(t)$ varies sinusoidally. In the season with high vector activity, the value of $\beta(t)$ increases and infection rate increases accordingly. Importantly, the figure also illustrates the reproduction number $\mathcal{R}_0(t)$ as an key epidemiological metric. As $\beta(t)$ increases due to favourable environmental conditions, $\mathcal{R}_0(t)$ also rises, indicating that the disease is more likely to spread rapidly within the population. The figure shows oscillatory behaviour for periodic rise and fall of infections induced by changes in $\beta(t)$ throughout the season. In classical epidemiological models the reproduction number is often considered as a constant, however, it is appropriate and useful to represent the reproduction number as a time varying parameter when the transmission rate $\beta(t)$ is explicitly time varying. This time-varying reproduction number, $\mathcal{R}_0(t)$, better reflects the reality of the risk of transmission. It may also include the effect of environmental change in transmission dynamics.

Numerical simulation

In this section, the numerical scheme using Lagranian piece-wise interpolation, simulations, and detailed explanation of the result thus obtained are carried out. For the proposed model (1), the initial hypothetical consideration of state variables using Fig. 2 and Table 2 data are $S(0) = 100$, $I(0) = 50$, $R(0) = 20$ and $V(0) = 700$. The parameters value are taken from Table 1. The scrub typhus infection disappears within half a week, thus short memory effect is associated by implementing fractional parameters closer to unity. Inducing AB-intergral to model (1) gives

$$\begin{aligned}
S(t) &= S(0) + \frac{nt^{n-1}\mathcal{M}_1(S,I,R,V,t)}{P(m)} + nQ(m)\int_0^t (t-l)^{m-1} l^{n-1}\mathcal{M}_1(S,I,R,V,l)\,dl,\\
It) &= I(0) + \frac{nt^{n-1}\mathcal{M}_2(S,I,R,V,t)}{P(m)} + nQ(m)\int_0^t (t-l)^{m-1} l^{n-1}\mathcal{M}_2(S,I,R,V,l)\,dl,\\
R(t) &= R(0) + \frac{nt^{n-1}\mathcal{M}_3(S,I,R,V,t)}{P(m)} + nQ(m)\int_0^t (t-l)^{m-1} l^{n-1}\mathcal{M}_3(S,I,R,V,l)\,dl,\\
V(t) &= V(0) + \frac{nt^{n-1}\mathcal{M}_4(S,I,R,V,t)}{P(m)} + nQ(m)\int_0^t (t-l)^{m-1} l^{n-1}\mathcal{M}_4(S,I,R,V,l)\,dl.
\end{aligned} \tag{9}$$

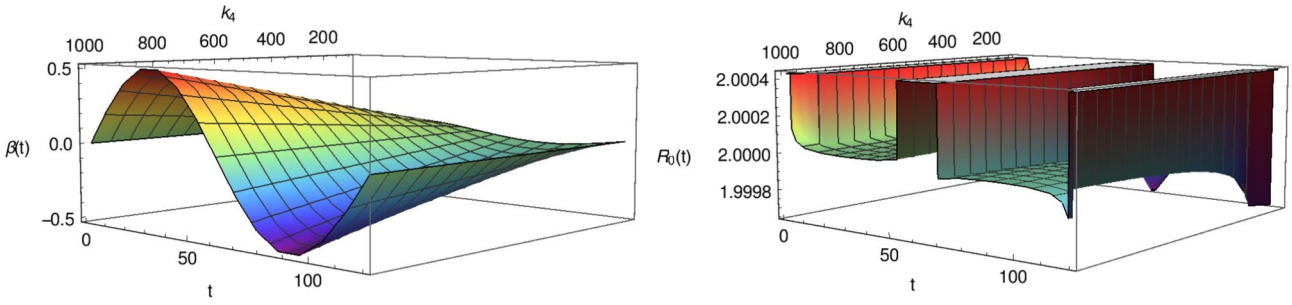

(a) Effect of season on infection transmission rate in human.

(b) Time dependent reproduction number.

Fig. 3. The effect of changing transmission rate $\beta(t)$ and reproduction number $\mathcal{R}_0(t)$ on the dynamics of the scrub typhus infection. The plotting of figures is done by cloud Mathematica in wolframcloud.com.

Further, t is replaced by t_{j+1} in the integrands of Eq. (9) and necessary adustments elsewhere in the same set of equations to get

$$\begin{aligned}
S^{j+1}(t) &= S(0) + \frac{nt_j^{n-1}\mathcal{M}_1\left(S^j, I^j, R^j, V^j, t_j\right)}{P(m)} \\
&\quad + nQ(m)\int_0^{t_{j+1}} (t_{j+1}-l)^{m-1} l^{n-1}\mathcal{M}_1\left(S, I, R, V, l\right) dl, \\
I^{j+1}(t) &= I(0) + \frac{nt_j^{n-1}\mathcal{M}_2\left(S^j, I^j, R^j, V^j, t_j\right)}{P(m)} \\
&\quad + nQ(m)\int_0^{t_{j+1}} (t_{j+1}-l)^{m-1} l^{n-1}\mathcal{M}_2\left(S, I, R, V, l\right) dl, \\
R^{j+1}(t) &= R(0) + \frac{nt_j^{n-1}\mathcal{M}_3\left(S^j, I^j, R^j, V^j, t_j\right)}{P(m)} \\
&\quad + nQ(m)\int_0^{t_{j+1}} (t_{j+1}-l)^{m-1} l^{n-1}\mathcal{M}_3\left(S, I, R, V, l\right) dl, \\
V^{j+1}(t) &= V(0) + \frac{nt_j^{n-1}\mathcal{M}_4\left(S^j, I^j, R^j, V^j, t_j\right)}{P(m)} \\
&\quad + nQ(m)\int_0^{t_{j+1}} (t_{j+1}-l)^{m-1} l^{n-1}\mathcal{M}_4\left(S, I, R, V, l\right) dl.
\end{aligned} \tag{10}$$

Now, from Eq. (10) we get more concise recursive relations which are given as follows:

$$\begin{aligned}
S^{j+1}(t) =& S(0) + \frac{nt_j^{n-1}\mathcal{M}_1\left(S^j, I^j, R^j, V^j, t_j\right)}{P(m)} \\
&+ nQ(m)\sum_{r=0}^{j}\int_{t_r}^{t_{r+1}} (t_{j+1}-l)^{m-1} l^{n-1}\mathcal{M}_1\left(S, I, R, V, l\right) dl, \\
I^{j+1}(t) =& I(0) + \frac{nt_j^{n-1}\mathcal{M}_2\left(S^j, I^j, R^j, V^j, t_j\right)}{P(m)} \\
&+ nQ(m)\sum_{r=0}^{j}\int_{t_r}^{t_{r+1}} (t_{j+1}-l)^{m-1} l^{n-1}\mathcal{M}_2\left(S, I, R, V, l\right) dl,
\end{aligned} \tag{11}$$

$$\begin{aligned}
R^{j+1}(t) =& R(0) + \frac{nt_j^{n-1}\mathcal{M}_3\left(S^j, I^j, R^j, V^j, t_j\right)}{P(m)} \\
&+ nQ(m)\sum_{r=0}^{j}\int_{t_r}^{t_{r+1}} (t_{j+1}-l)^{m-1} l^{n-1}\mathcal{M}_3\left(S, I, R, V, l\right) dl, \\
V^{j+1}(t) =& V(0) + \frac{nt_j^{n-1}\mathcal{M}_4\left(S^j, I^j, R^j, V^j, t_j\right)}{P(m)} \\
&+ nQ(m)\sum_{r=0}^{j}\int_{t_r}^{t_{r+1}} (t_{j+1}-l)^{m-1} l^{n-1}\mathcal{M}_4\left(S, I, R, V, l\right) dl.
\end{aligned} \tag{12}$$

with $t_0 = 0$.

If $\psi = t_{r+1} - t_r$, then we discritize the Eq. (11) to get (for the iterative scheme we take $t_{j+1} = 300$ and $\psi = 0.5$)

$$
\begin{aligned}
S^{j+1}(t) &= S(0) + \frac{nt_j^{n-1}\mathcal{M}_1\left(S^j, I^j, R^j, V^j, t_j\right)}{P(m)} \\
&+ \frac{s\psi^m}{\mathcal{N}(m)\Gamma(m+2)}\sum_{r=1}^{j}[t_r^{n-1}\mathcal{M}_1(t_r, S^r, I^r, R^r, V^r)\times((j+1-r)^m\,(j-r+2+m) \\
&- (j-r)^m\,(j-r+2+2m)) - t_{r-1}^{n-1}\mathcal{M}_1(t_r, S^{r-1}, E^{r-1}, V^{r-1}, I^{r-1})\times((j-r+1)^{m+1} \\
&- (j-r)^m(j-r+1+m))], \\
I^{j+1}(t) &= I(0) + \frac{nt_j^{n-1}\mathcal{M}_2\left(S^j, I^j, R^j, V^j, t_j\right)}{P(m)} \\
&+ \frac{s\psi^m}{\mathcal{N}(m)\Gamma(m+2)}\sum_{r=1}^{j}[t_r^{n-1}\mathcal{M}_2(t_r, S^r, I^r, R^r, V^r)\times((j+1-r)^m\,(j-r+2+m) \\
&- (j-r)^m\,(j-r+2+2m)) - t_{r-1}^{n-1}\mathcal{M}_2(t_r, S^{r-1}, E^{r-1}, V^{r-1}, I^{r-1})\times((j-r+1)^{m+1} \\
&- (j-r)^m(j-r+1+m))], \\
R^{j+1}(t) &= R(0) + \frac{nt_j^{n-1}\mathcal{M}_3\left(S^j, I^j, R^j, V^j, t_j\right)}{P(m)} \\
&+ \frac{s\psi^m}{\mathcal{N}(m)\Gamma(m+2)}\sum_{r=1}^{j}[t_r^{n-1}\mathcal{M}_3(t_r, S^r, I^r, R^r, V^r)\times((j+1-r)^m\,(j-r+2+m) \\
&- (j-r)^m\,(j-r+2+2m)) - t_{r-1}^{n-1}\mathcal{M}_3(t_r, S^{r-1}, E^{r-1}, V^{r-1}, I^{r-1})\times((j-r+1)^{m+1} \\
&- (j-r)^m(j-r+1+m))], \\
V^{j+1}(t) &= V(0) + \frac{nt_j^{n-1}\mathcal{M}_4\left(S^j, I^j, R^j, V^j, t_j\right)}{P(m)} \\
&+ \frac{s\psi^m}{\mathcal{N}(m)\Gamma(m+2)}\sum_{r=1}^{j}[t_r^{n-1}\mathcal{M}_4(t_r, S^r, I^r, R^r, V^r)\times((j+1-r)^m\,(j-r+2+m) \\
&- (j-r)^m\,(j-r+2+2m)) - t_{r-1}^{n-1}\mathcal{M}_4(t_r, S^{r-1}, E^{r-1}, V^{r-1}, I^{r-1})\times((j-r+1)^{m+1} \\
&- (j-r)^m(j-r+1+m))].
\end{aligned}
\tag{13}
$$

Results and Interpretation

This section comprises of scientific translation of the Figs. 4, 5, 6. We display the computational work performed on mathematical model (1) mentioned in previous section. Using the Lagrange's interpolation scheme, the model was solved under the parameter extents represented in Table 1. These simulations are intended to show the dynamic behaviour of the system for operating conditions.

In Fig. 4, each sub-plot illustrates the time evolution of the host-infected population for three fractional parameter values $(m = n = 0.98, 0.96, 0.94)$ under increasing amplitude values: Further, we have assumed the following four scenarios for the k_4 parameter: (a) $k_4 = 100$, (b) $k_4 = 500$, (c) $k_4 = 1000$. Consequently, the greater the fractional parameters, the faster the transmission and earlier the peaks in the infected population, and higher values of the amplitude increases the impact of the environmental factor and results in sharper and swifter infection rate. The plots further show the impact of memory effects and environmental conditions in governing the spreading dynamics of scrub typhus.

i) Figure 4a: Initially the infected population increases for all the values of *m* and *n*. The peak point is as follows; the population reaches its highest point in the given time at which the fractional values are possible. We see that for $m = n = 0.98$ infection peaks earlier, where as when *m* and *n* decreases (0.96 to 0.94), the infection peaks later. The plot under consideration indicates that increase of the fractional parameters $(m = n = 0.98)$ leads to growth of the infected population and its peak earlier. On the other hand, at lesser *m* and *n* values, infected population is growing at a slower pace, and it takes longer time for it to make that growth rate as at the maximum.
ii) Figure 4b: This plot is similar to Fig. (4a), but the oscillation is with greater amplitude, which means that the influence of environment factors such as temperature or vector activity on transmission is more significant. The host-infected population size increases at a faster rate than in the first plot because of the significant oscillation. The peaks still occur at the earlier time for larger fractional parameters *m* and *n* values, however, infected population reaches higher maxima in this case because of a dominance of environmental forces described by k_4.
iii) Figure 4c: The plot shows an even greater impact of environmental factors as opposed to the social factors in transmitting diseases. The size of the infected population has its maximum at significantly earlier time than the susceptible population, especially for higher *m* and *n*. In this case, the peak infected population rises much higher to incorporate for a situation where the external circumstantial factors positively influence and boosts the rate of infection such as favourable conditions in the breeding place of vectors.

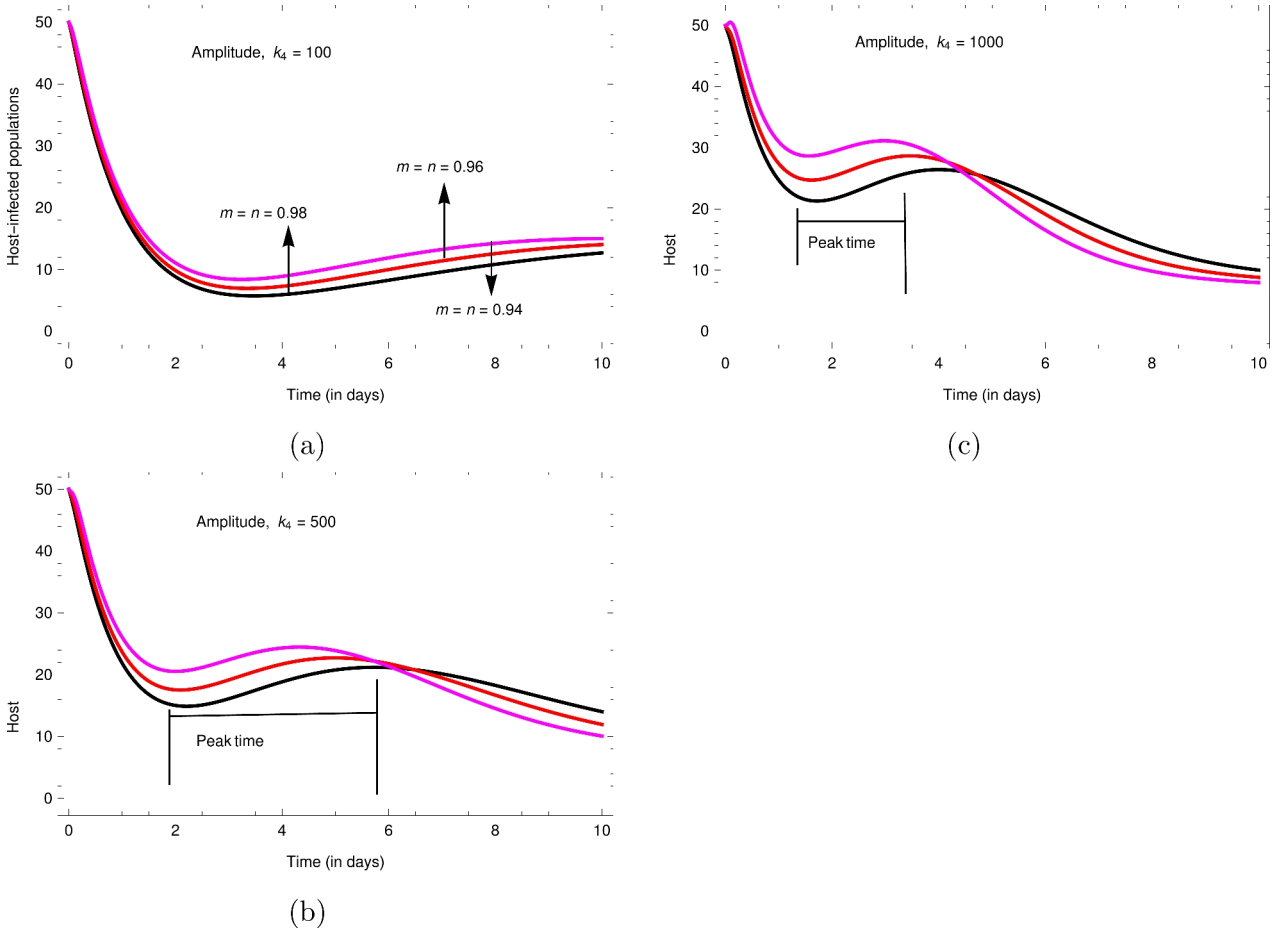

Fig. 4. Host-infected population oscillations with respect to different fractional parameters *m* and *n* together with distinct environmental amplitudes k_4, and $\beta_0 = \frac{1}{5000}$ (from Table 1).

Figure (5) individually describes the effect that the fractional parameters and the environmental conditions play in affecting herd immunity thresholds, the infection dynamics, and the total disease spread by the host population.

i) Figure 5a: The plot shows how the number of susceptible individuals decrease and the number of recovered individuals increase with time. For faster recovery, the values of *m* and *n* (closer to 1) give faster transmission and recovery due to the population memory effect (longer influence from past infection rates). The fractional parameters meet points H_1, H_2 and H_3 where herd immunity is attained. Because of faster disease spread, these thresholds are lower, and they happen at earlier times, for higher *m* and *n* values. The larger *m* and *n* are, the more important is the memory effects in population, which means that past infections have significant impact on the current disease dynamics. The result is a speedier depletion of people in the population that are susceptible and a speedier build up of people recovered, meaning that immunity spreads quickly from one person to the next.
ii) Figure 5b: For all fractional values, even due to higher amplitude ($k_4 = 500$) implying stronger environmental impacts (favorable breeding conditions for mite), the disease spread is more rapid compared to the other fractional values. As transmission gets faster, the recovery rate grows. In particular, the susceptibility is solved faster than in Fig. (5a), in particular for $m = n = 0.98$. Recovery builds up very quickly for larger *m* and *n*, with the curves of growth steeper than $m = n = 0.94$. Because of the increased transmission rate, higher thresholds (more recovered individuals) are achieved.
iii) Figure 5c: The host-susceptibles quickly decline for all values of *m*, *n* even more rapidly than in Fig. (5b). It is an extremely aggressive spread of the disease owing to good environmental conditions (high k_4). The faster loss of infection is also observed in the recoveries. The recovered populations rise more quickly for *m* and *n* near to 1. Particularly for $m = n = 0.98$, where almost all of the susceptible population is converted to the recovered population, the thresholds are reached very early. In these cases, even for $m = n = 0.94$, the recovery process is fast under strong environmental coupling.
iv) Figure 5d: The infected populations vary over time, always peaking at different times - depending on *m* and *n*. The peaks in such cases come earlier and sharper. Infections resolve, and the recoveries build, in inverse relationship with the infected population. On the other hand, turning points (peaks in the infected popula-

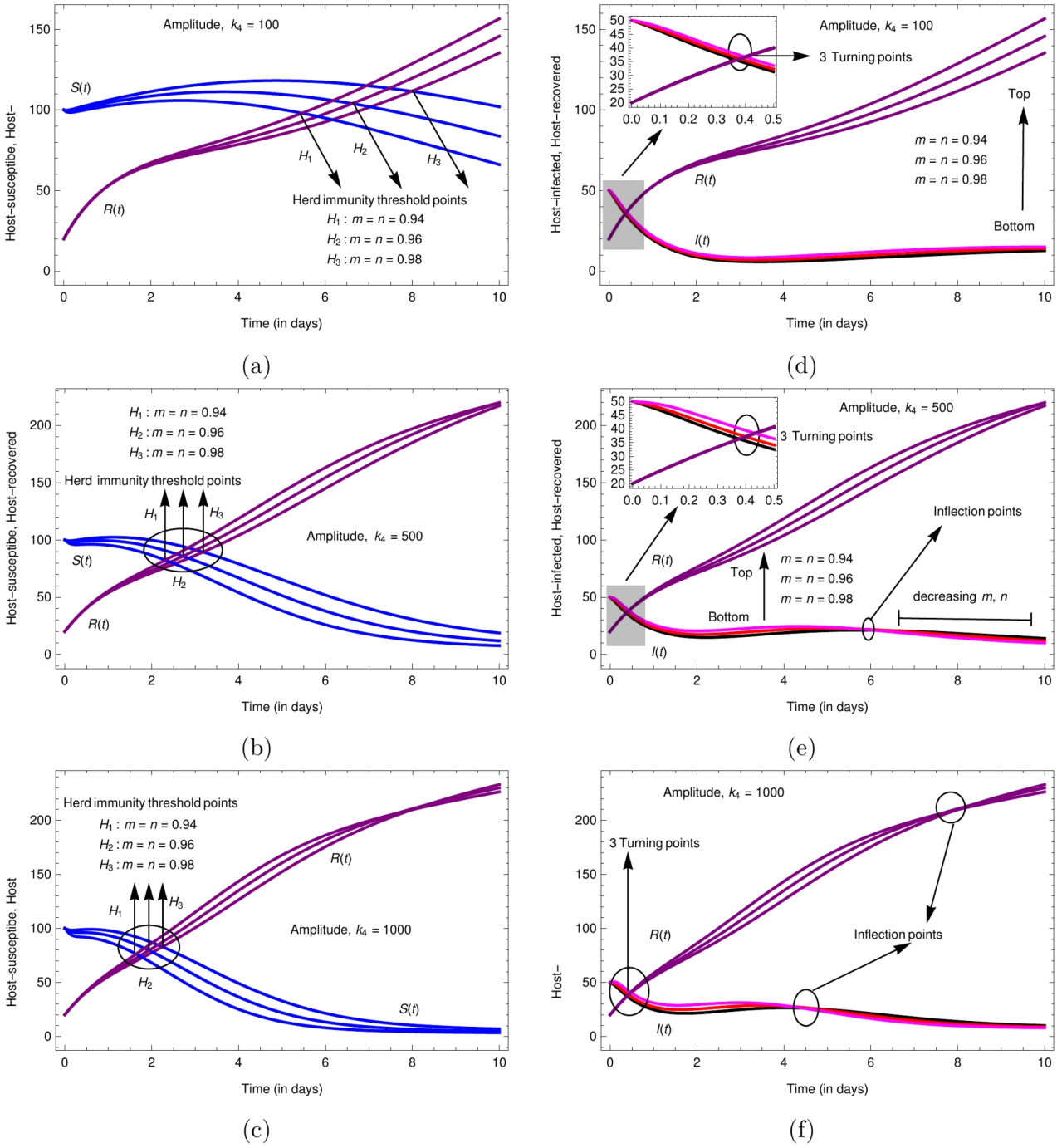

Fig. 5. Herd immunity thresholds and turning points in host-susceptible, host-recovered and host-infected population dynamics with fractional parameters m and n and various environmental amplitudes k_4.

tion), earlier for higher m and n, correspond to faster disease progression. Higher m and n are also found to be more inflection points (change in growth rate of infection) or sharper peaks.

v) Figure 5e: The infected population grows faster and reaches a higher peak earlier than in Fig. (5d) due to stronger environmental influence. Infections are easier to resolve and recovery accelerates. Faster transmission makes turning and inflection points sharper and happen earlier. Both infection, and more quickly, but also recovery processes, are sped up by environmental factors, resulting in earlier and stronger infection peaks. What this means, is that the interval of time at which public health measures should be intensified is during the seasons that have higher vector activity to avoid rapid outbreaks.

vi) Figure 5f: For all values of m and n, the infected population peaks very early, corresponding to a very aggressive outbreak. The rate that recoveries occur is more or less simultaneous with the drop in infections, and in large numbers relative to the number of infections themselves. Under the strong environmental impact,

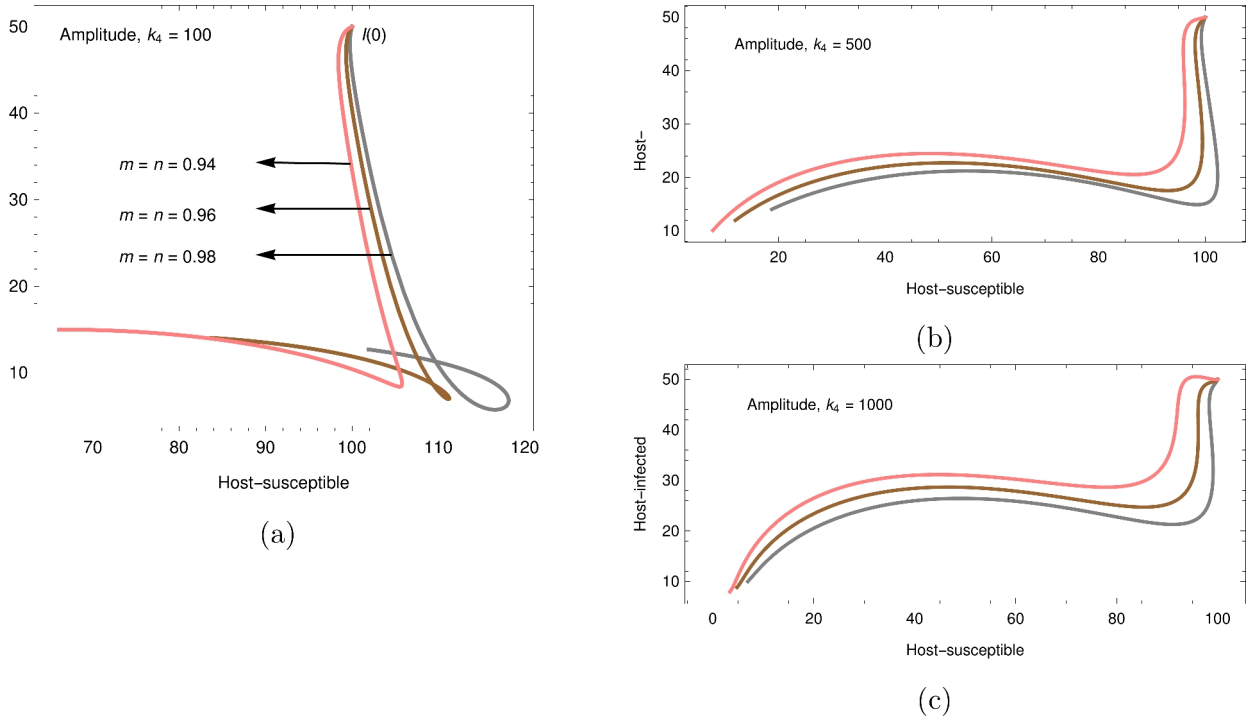

Fig. 6. Varying fractional parameters m and n with different environmental amplitudes k_4 and the relationship between host-susceptible and host-infected populations.

the infection peaks are almost instantaneous. Rapid response strategies are necessary to emergency manage such aggressive outbreaks because of the extreme environmental factors that cause an outbreak to reach its peak almost immediately.

In Fig. (6) the phase plane trajectories of the host-susceptible $S(t)$ and host-infected $I(t)$ population as a function of a variety of fractional parameters m and n, and environmental amplitudes k_4 are presented. The resulting phase plane diagrams expose the disease logic through the population as susceptible individuals are progressing through the population being become infected and how the memory effects (fractional parameters) and environmental effects (amplitude) impact the outbreak dynamics.

The dynamics of the system are captured in each sub-plot for a given amplitude k_4, and fractional parameters m, n that control the system's memory effects, how past infection rates influence current dynamics.

i) Figure 6a: The curves indicate the ascent of the number of infected individuals from decrease in the number of susceptible individuals matching the time series in which susceptibles succumbed to the disease transmission process. For higher fractional values $(m = n = 0.98)$, the infection grows faster than for the prior simulations: it takes shorter time to see the drop in the susceptible population and the rise in the infected population. The steeper curve for indicate this idea. In particular, disease spreads more slowly for smaller fractional values $(m = n = 0.94)$, in which the susceptible population declines gradually, and the infected population grows slowly.
ii) Figure 6b: For a $k_4 = 500$, which, characterizing stronger environmental influences, the infection propagates more quickly over higher fractional values. In the case of $m = n = 0.98$, the infection curve steepens, meaning the disease spreads really fast, and quickly drops the susceptible population and increases infections. Even for $m = n = 0.94$ the infection spreads less quickly than in plot Fig. 6a because of the increased environmental influence.
iii) Figure 6c: The most aggressive spread is from the highest amplitude $k_4 = 1000$, which may suggests peak mite activity due to best weather conditions. For higher fractional values, even the susceptible population gets overwhelmed by the fast spread of infection in such cases. Timely intervention has been highlighted on this plot. The outbreak can escalate very quickly if the environmental conditions for the disease vector are very favorable but if public health measures are not instituted promptly, control is difficult.

Conclusions

Based upon 13 years of data (2010-2022), this research develops a novel mathematical model of scrub typhus disease dynamics in Northeast India. Using the Atangana-Baleanu fractal-fractional operator, the model captures the seasonal transmission patterns of disease in a robust fashion, allowing us to understand the reported cases.

Novelty and significance: The application of fractal-fractional derivative to modelling infectious diseases, with scrub typhus as the most prominant example, is an advance in epidemiology. This approach is beyond traditional

integer order models, utilizing memory effects and describing the complex real world behavior of vector borne diseases more accurately. This is an especially powerful model, in that it can integrate both biologically and environmentally relevant factors, such as temperature, humidity, and mite activity, for regions with seasonal climate variation. In addition, the fractional parameters give insight on how past infection rates affect current dynamics leading to more refined predictions of future outbreaks. This is important for public health planning as it identifies the time when transmission risk is highest, i.e. the rainy season when mite activity is at its peak.

Utility of the model: The greatest utility of the model is the ability to simulate the spread of scrub typhus under a variety of environmental conditions, as well as intervention strategies. This model addresses a crucial gap in Northeast India's epidemiological data in terms of disease dynamics by accounting for under-reporting factors. An existence-uniqueness analysis, grounded in the theory of fixed points, demonstrates that the model is mathematically sound and will predict reliably. Furthermore, the model demonstrates the impact of memory effects in infectious disease transmission, where infection rates cannot only be a function of current conditions, but also depend on historical information. This feature lends itself to more long term planning and response strategy for disease outbreaks.

The fractional parameters are compared and show that higher values have faster transmission and earlier peaks in the infected population, while lower values cause a delay in outbreak. This underscores the importance of drawing on scientific evidence for rapid response, especially in places where environmental factors, such as increased humidity and temperature, can make the disease spread even worse. Finally, the study includes a seasonal variation component, with a sinusoidal infection transmission rate, and this realism is an important part of how climatic factors impact scrub typhus outbreaks. However, the model's predictive capability for intra-seasonal fluctuations enhances the usefulness of this tool by public health officials to trigger targeted interventions in high risk periods. For a developing country like India, maintenance of neglected tropical disease data like scrub typhus is very tedious job but central and state ministry together must declare standard operating procedure to collect survey reports for such cases in much better way. Like the works penned in references[44,45], the authors would like to extend the work in future with more real data.

Data availability

The data used in this research are cited as a part of the article and no other additional data source are required.

Received: 30 October 2024; Accepted: 21 March 2025
Published online: 28 March 2025

References

1. Mohapatra, R. K. et al. Linking the increasing epidemiology of scrub typhus transmission in India and South Asia: Are the varying environment and the reservoir animals the factors behind?. *Front. Tropical Dis.* **5**, 1371905 (2024).
2. WHO. Who recommended surveillance standards, 1999. [Online; accessed 25-September-2024].
3. Trent, B., Fisher, J. & Soong, L. Scrub typhus pathogenesis: Innate immune response and lung injury during orientia Tsutsugamushi infection. *Front. Microbiol.* **10**, 2065 (2019).
4. Costa, C. et al. Imported scrub typhus in Europe: Report of three cases and a literature review. *Travel Med. Infect. Dis.* **42**, 102062 (2021).
5. Roberts, T. et al. A spatio-temporal analysis of scrub typhus and murine typhus in laos; Implications from changing landscapes and climate. *PLoS Negl. Tropical Dis.* **15**(8), e0009685 (2021).
6. Tran, H. T. D. et al. Ecological and behavioural risk factors of scrub typhus in central Vietnam: A case-control study. *Infect. Dis. Poverty* **10**, 1–14 (2021).
7. Wangrangsimakul, T. et al. The estimated burden of scrub typhus in Thailand from national surveillance data (2003–2018). *PLoS Negl. Tropical Dis.* **14**(4), e0008233 (2020).
8. Konyak, B. M. et al. Scrub typhus in northeast India: Epidemiology, clinical presentations, and diagnostic approaches. *Transac. Royal Soc. Trop. Med. Hygiene* **118**(3), 206–222 (2023).
9. Richards, A. L. & Jiang, J. Scrub typhus: Historic perspective and current status of the worldwide presence of orientia species. *Tropical Med. Infect. Dis.* **5**(2), 49 (2020).
10. Khan, H. et al. On a fractal-fractional-based modeling for influenza and its analytical results. *Qual. Theory Dyn. Syst.* **23**(2), 70 (2024).
11. Ahmed, S., Azar, A. T., Abdel-Aty, M., Khan, H. & Alzabut, J. A nonlinear system of hybrid fractional differential equations with application to fixed time sliding mode control for leukemia therapy. *Ain Shams Eng. J.* 102566 (2024).
12. Zafar, Z. U. A. et al. Impact of public health awareness programs on covid-19 dynamics: A fractional modeling approach. *FRACTALS (fractals)* **31**(10), 1–20 (2023).
13. Asamoah, J. K. K. Fractal-fractional model and numerical scheme based on newton polynomial for Q fever disease under atangana-baleanu derivative. *Results Phys.* **34**, 105189 (2022).
14. Addai, E., Zhang, L., Asamoah, J. K. & Essel, J. F. A fractional order age-specific smoke epidemic model. *Appl. Math. Model.* **119**, 99–118 (2023).
15. Asamoah, J. K. K. et al. A fractional mathematical model of heartwater transmission dynamics considering nymph and adult amblyomma ticks. *Chaos, Solitons & Fractals* **174**, 113905 (2023).
16. Asamoah, J. K. K. & Sun, G.-Q. Fractional caputo and sensitivity heat map for a gonorrhea transmission model in a sex structured population. *Chaos Solitons Fractals* **175**, 114026 (2023).
17. Ahmad, I., Ali, I., Jan, R., Idris, S. A. & Mousa, M. Solutions of a three-dimensional multi-term fractional anomalous solute transport model for contamination in groundwater. *Plos One* **18**(12), e0294348 (2023).
18. Naik, P. A., Yeolekar, B. M., Qureshi, S., Yeolekar, M. & Madzvamuse, A. Modeling and analysis of the fractional-order epidemic model to investigate mutual influence in hiv/hcv co-infection. *Nonlinear Dyn.* 1–32 (2024).
19. Atangana, A. Fractal-fractional differentiation and integration: Connecting fractal calculus and fractional calculus to predict complex system. *Chaos Solitons Fractals* **102**, 396–406 (2017).
20. Thiriot, J., Liang, Y., Fisher, J., Walker, D. H. & Soong, L. Host transcriptomic profiling of cd-1 outbred mice with severe clinical outcomes following infection with orientia tsutsugamushi. *PLoS Negl. Tropical Dis.* **16**(11), e0010459 (2022).
21. Shah, N. N. H. et al. Enhancing public health strategies for tungiasis: A mathematical approach with fractional derivative. *AIMS Bioeng.* **10**(4), 384–405 (2023).

22. Kwak, J. et al. Scrub typhus incidence modeling with meteorological factors in South Korea. *Int. J. Environ. Res. Public Health* **12**(7), 7254–7273 (2015).
23. Min, K.-D. & Cho, S.-I. Mathematical modeling for scrub typhus and its implications for disease control. *J. Korean Med. Sci.* **33**, 12 (2018).
24. Yao, H. et al. The scrub typhus in mainland china: Spatiotemporal expansion and risk prediction underpinned by complex factors. *Emerg. Microb. Infect.* **8**(1), 909–919 (2019).
25. Bondarenko, V., Mazzega, P. & Lajaunie, C. Predictability of scrub typhus incidences time series in Thailand. *Eng. Proc.* **5**(1), 44 (2021).
26. D'Cruz, S., Sreedevi, K., Lynette, C., Gunasekaran, K. & Prakash, J. A. J. Climate influences scrub typhus occurrence in Vellore, Tamil nadu, India: Analysis of a 15-year dataset. *Sci. Rep.* **14**(1), 1532 (2024).
27. Peng, P.-Y. et al. Epidemiologic changes of a longitudinal surveillance study spanning 51 years of scrub typhus in mainland china. *Sci. Rep.* **14**(1), 3138 (2024).
28. Cheryl Lynnette, S. et al. Scrub typhus diagnostics: The present and the future. *Zoonoses* **4**(1), 990 (2024).
29. Clinical overview of scrub typhus: National center for emerging and zoonotic infectious diseases (ncezid). https://www.cdc.gov/typhus/hcp/clinical-overview/clinical-overview-of-scrub-typhus.html#:~:text=Most%20patients%20have%20thrombocytopenia%20and,severe%20than%20the%20initial%20presentation., 2024. [Online; accessed 14-October-2024].
30. Paun, M.-A., Paun, V.-A. & Paun, V.-P. Acoustic fractional propagation in terms of porous xerogel and fractal parameters. *Gels* **10**(1), 83 (2024).
31. Kalachev, L., Graham, J. & Landguth, E. L. A simple modification to the classical sir model to estimate the proportion of under-reported infections using case studies in flu and covid-19. *Infect. Dis. Model.* (2024).
32. Shocket, M. S., Caldwell, J. M., Huxley, P. J., Lippi, C. A., Windram, F. A., & Keyel, A. C. Modelling the effects of climate and climate change on transmission of vector-borne disease. In *Planetary health approaches to understand and control vector-borne diseases*. Wageningen Academic, pp. 253–318 (2023)
33. Giménez-Mujica, U., Velázquez-Castro, J. & Anzo-Hernández, A. Final size of the epidemic for metapopulation vector-borne diseases. *J. Math. Anal. Appl.* **526**(1), 127200 (2023).
34. Young, M. J. & Fefferman, N. H. A 'portfolio of model approximations' approach to understanding invasion success with vector-borne disease. *Math. Biosci.* **358**, 108994 (2023).
35. Gao, D. & Cao, L. Vector-borne disease models with lagrangian approach. *J. Math. Biol.* **88**(2), 22 (2024).
36. Wang, K., Zhao, H. & Wang, H. Asymptotic profiles of a spatial vector-borne disease model with Fokker-Planck-type diffusion. *Stud. Appl. Math.* **152**(4), 1305–1337 (2024).
37. Anwar, M. N. et al. Mathematical models of plasmodium vivax transmission: A scoping review. *PLOS Comput. Biol.* **20**(3), e1011931 (2024).
38. Ferraguti, M. Mosquito species identity matters: Unraveling the complex interplay in vector-borne diseases. *Infect. Dis.* 1–12 (2024).
39. Qiang, L. & Zhang, X. A reaction-diffusion vector-borne disease model with incubation period in almost periodic environments. *Nonlinear Anal. Real World Appl.* **79**, 104103 (2024).
40. Saha, P., Sikdar, G. C., Ghosh, J. K. & Ghosh, U. Disease dynamics and optimal control strategies of a two serotypes dengue model with co-infection. *Math. Comput. Simul.* **209**, 16–43 (2023).
41. Ahmed, K. I., Adam, H. D., Youssif, M. & Saber, S. Different strategies for diabetes by mathematical modeling: Applications of fractal-fractional derivatives in the sense of atangana-baleanu. *Results Phys.* **52**, 106892 (2023).
42. Selvam, A. et al. Ulam-hyers stability of tuberculosis and covid-19 co-infection model under Atangana-Baleanu fractal-fractional operator. *Sci. Rep.* **13**(1), 9012 (2023).
43. Garba, S. M. & Gumel, A. B. Effect of cross-immunity on the transmission dynamics of two strains of dengue. *Int. J. Comput. Math.* **87**(10), 2361–2384 (2010).
44. Meetei, M. Z. et al. Analysis and simulation study of the hiv/aids model using the real cases. *Plos One* **19**(6), 0304735 (2024).
45. Khan, M. A., DarAssi, M. H., Ahmad, I., Seyam, N. M. & Alzahrani, E. The transmission dynamics of an infectious disease model in fractional derivative with vaccination under real data. *Comput. Biol. Med.* **181**, 109069 (2024).

Acknowledgements

The Researchers would like to thank the Deanship of Graduate Studies and Scientific Research at Qassim University for financial support (QU-APC-2025).

Author contributions

B.D. and M.S. conceptualized the work. B.D. wrote the manuscript. B.D. and M.S. analyzed the results. M.S. initiated funding. All authors reviewed the manuscript.

Declarations

Competing interests

The authors declare no competing interests.

Ethics approval

During the research, this article does not contain any kind of experiments with humans as well as animals by the authors.

Additional information

Correspondence and requests for materials should be addressed to M.S.

Reprints and permissions information is available at www.nature.com/reprints.

Publisher's note Springer Nature remains neutral with regard to jurisdictional claims in published maps and institutional affiliations.